Solid Freeform Fabrication 2019: Proceedings of the 30th Annual International Solid Freeform Fabrication Symposium – An Additive Manufacturing Conference
Reviewed Paper

DEVELOPMENT OF A CIRCULAR 3S 3D PRINTING SYSTEM TO EFFICIENTLY FABRICATE ALUMINA CERAMIC PRODUCTS

Jia–Chang Wang[1,2] Ph.D., Hitesh. D[3]*

[1] Department of Mechanical Engineering, National Taipei University of Technology; jcw@mail.ntut.edu.tw
[2] Additive Manufacturing Center for Mass Customization Production, National Taipei University of Technology, Taipei, Taiwan
[3] College of Mechanical & Electrical Engineering, National Taipei University of Technology; iamhitesh89@gmail.com

Abstract

The Solvent based Slurry Stereolithography (3S) system has the capability of fabricating high quality objects using high performance ceramic (HPC) material. The 3S system is able to fabricate intrinsic features without supporting structures; while its downsides exhibit consuming lot of time (30 sec/layer) for fabrication compared to other DLP apparatuses and low efficiency raw material consumption. A new system named as Circular - 3S (C3S) is developed by adapting the 3S technology to improve the fabrication process. It consists of multiple DLP and a circular platform where a paving blade paves the slurry in a circular manner. The demonstrated system has increased the production rate to 200% with printing speed of 15sec/layer. In this paper, the development of the C3S system is presented by simultaneously displaying the capabilities and raw material efficiency of the new C3S system.

Keywords: *Additive manufacturing, 3D printing, ceramics, slurry, 3S, ceramics, alumina*

1. Introduction

Manufacturing and prototyping of ceramic components in a small-scale can increase the expenses for the molds and processing. Particularly for the new and complex designs, it is difficult to adapt to produce in a smaller volume at an economical price. Additive manufacturing (AM) can cut down the processing expenses by reducing the number of steps down to only a few. AM allows for the production of structures with complex topologies, while also allowing for the usage of different materials, including metals and alloys (Frazier, 2014), ceramics (Wang, Dommati and Hsieh, 2019), polymers and plastics (Ligon *et al.*, 2017; Dizon *et al.*, 2018).

AM with ceramics has existed since the year 1986 (Lee *et al.*, 1986), in which a photopolymerized tape casting process was described. In addition to tape casting, laser scanning and digital light projection are also very common methods of fabricating ceramic products. In recent times, there have been major developments in building High Performance Ceramic (HPC) materials with intrinsic features while preserving the thermal, mechanical and corrosive resistance properties of the structure materials. AM systems are now able to build functional grade dense ceramic materials in small scale. (Tang, Chiu and Yen, 2011; Liu *et al.*, 2013; Wang, 2013; Schwentenwein and Homa, 2015; He *et al.*, 2018; Hu *et al.*, 2018). Although most of the systems are capable of fabricating the functional grade HPC objects, they tend to exhibit low efficiency in the overall process and are limited to small volumes of parts.

The Lithography based Ceramic Manufacturing (LCM) based process by Lithoz GmbH (Schwentenwein and Homa, 2015), is a commercial system claims to fabricate 99.3% dense Alumina (Al) objects with 427MPa at 30 μm resolution and maximum volume of 76.8 × 43.2 mm in length and width. The CeraFab 7500 system claims to print up to 100 layers/ hour, i.e. 37.5 sec/layer, and the CeraFab S65 system claims to print up to 150 layers/hour, i.e. 24 sec/layer. This enables users to fabricate an 8mm thick object with a layer resolution of 25 μm within 3.2 hours and 2 hours respectively.

The 3S system developed to fabricate HPC materials is able to fabricate tiny features as small as several hundred microns (Wang, 2013; Wang and Dommati, 2018). However, the 3S system has a build volume of only 57.6 × 32.4 mm in length and width. The ratio for the build volume to the amount of slurry utilized in the 3S system is extremely high which leads to low efficiency of the system. The printing speed of the 3S system is 30 sec/layer.

Within industrial applications, it is important to optimize the fabrication time to reduce the wait time and increase productivity. The first 3S system has been improved to a new process called the Circular 3S system (C3S), in which the platform has a circular build plate and the cycle time for each layer is cut down to half the previous time. By adding another DLP system, the productivity has been multiplied to twice that of the single DLP system. In this paper, a new C3S system apparatus is built and compared to the previous 3S systems and other commercial systems available on the market. The samples 3D printed using C3S system are subjected to sintering and characterized by their flexural strength, density, surface roughness, and shrinkage rate.

2. Circular Solvent based Slurry Stereolithography (C3S) system

The C3S system follows the same working principle as the 3S system. The slurry is deposited on the build platform, the paving blade paves the slurry uniformly in a circular manner and the DLP system projects the blue light to cure the deposited layer. These steps are repeated until the green parts are formed. The obtained green parts are cleaned under the running water to remove the uncured residual slurry as a part of post processing. The post-processed objects are then sintered at up to 1600 ℃ to form completely dense ceramic objects.

2.1. Slurry formulation

The slurry is formulated using structure material, solvent, photo-curable resin, dispersant, and dye. The solvent used in this process is methanol while alumina is used as a structure material. The solvent is used to increase the viscosity of the slurry in order to enable homogenous distribution of alumina particles. An orange dye is used as a coloring agent to control the light rays' penetration during the curing process.

2.2. C3S apparatus

The C3S apparatus mainly consists of the following subsystems:

1) DLP system
2) Build platform
3) Rotating paving blade

4) Electronics control system
5) Human to Machine interface

The whole system is built into a closed cabinet with continuous air circulation and filters to avoid the surrounding dust. The layout of the C3S system is shown in Figure 1.

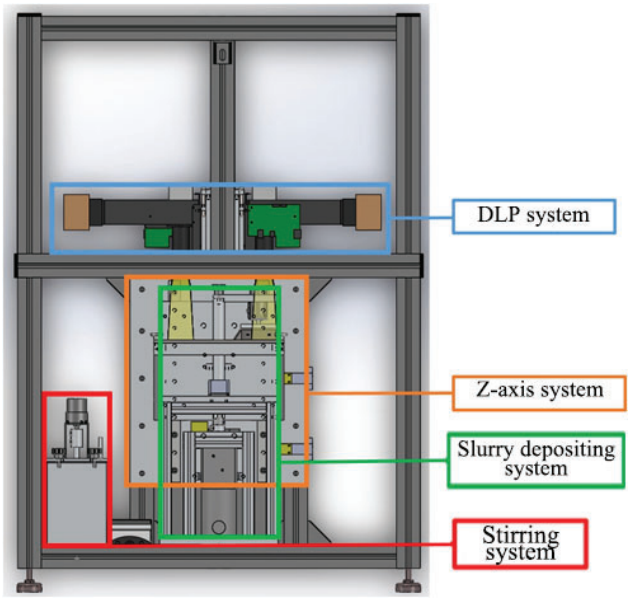

Figure 1: Layout of C3S system

2.2.1. DLP system

The C3S apparatus is able to host more than one DLP system in order to increase the productivity. In this present apparatus, two DLP systems are installed. However, the current setup is built to enable up to six projectors. Meaning, the productivity can be directly increased up to 6 times. Six different build volumes can be utilized to fabricate green parts. Figure 2 shows the NVM UV engine used in this process.

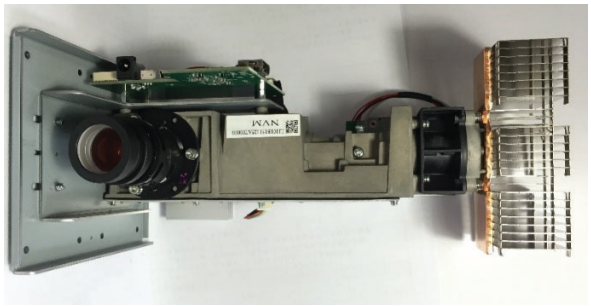

Figure 2: NVM UV Engine

The NVM UV engine is 2K resolution, naked body type setup that is compact in size. Hence, it is easy to accommodate multiple of such DLP systems.

2.2.2. Build platform

The build platform in this apparatus is a stainless steel square cut non-erosive plate on which the slurry is paved in a circular ring. The circular shape enables the slurry to pave over the surface continuously without letting it go waste, which is unlike the old 3S system where the excess slurry that is deposited for each layer goes waste. The build platform is setup with a linear actuator to carry it decremented or incremented in the Z-axis. Figure 3 shows the layout of the circular platform with up to 6 DLP configurations. In this paper, the P2 and P5 areas are used for exposing masking light on the slurry ring with two DLP systems.

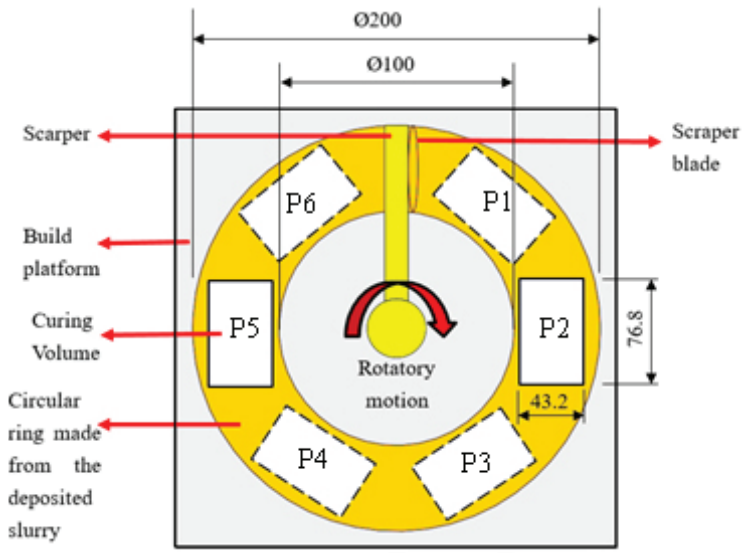

Figure 3: Build platform with circular paving

2.2.3. Rotating paving blade

The paving blade is used to pave the slurry into the circular ring over the build platform. It rotates continuously at a controlled speed. The paving blade design is as shown in the figure 4 (a), while Figure 4 (b) represents the setup of the paving blade in the apparatus.

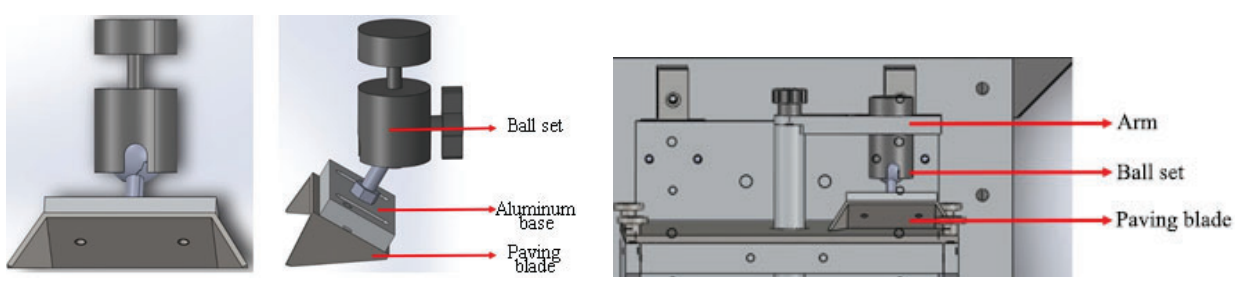

(a) (b)

Figure 4: (a) Paving blade design (b) Paving blade setup

2.2.4. Electronics control system

The C3S apparatus consists of a slurry dispensing system, a stirring system within the slurry tank, and an electronic control system that controls the whole setup.

The slurry dispensing system collects the slurry from the slurry tank through a pump and disperses it over the build platform. The pump motor speed is controlled in open loop and the input pulses are fixed to maintain the equal proportion of the slurry to be dispensed for every layer. The stirring system in the slurry tank is required to keep the slurry homogenous

In this setup, an open source Arduino board is used as the motherboard to control the Z-axis motion, paving blade motor control, masking light ON/OFF control, stirring motor ON/OFF, and the slurry dispensing pump. Figure 5 (a) and (b) shows the stirring system and the electronics control system.

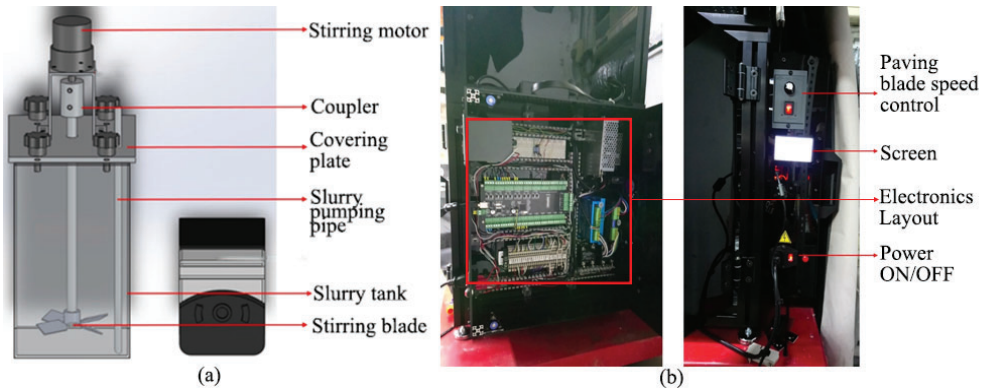

Figure 5: (a) Stirring system (b) Electronics layout

2.2.5. Human Machine Interface

An interface is developed to control the apparatus and feed the geometric codes to the machine from the computer. The interface is integrated with a slicing code that can directly slice the 3D file and send the control commands to the machine. The interface is as shown in the figure 6.

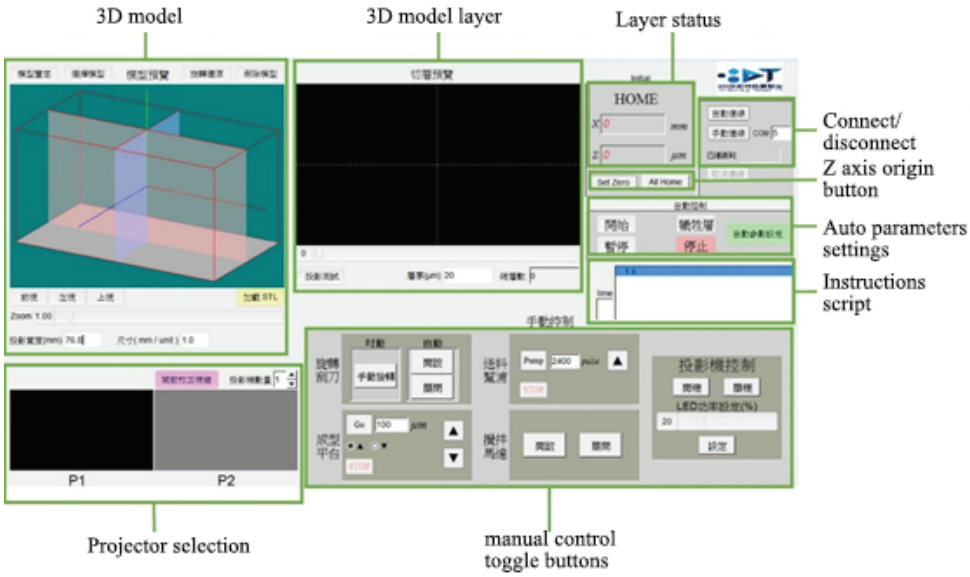

Figure 6: Interface layout

2.3. Fabrication of green parts

3D models and desired print parameters are fed to the user interface in Figure 6, which sends the information to the machine, which fabricates green parts layer-by-layer. The layer resolution that is possible in this apparatus is between the ranges of 10 – 50 µm range. With a recommended layer resolution of 20 µm and pixel resolution of 30 µm, the green parts can be fabricated at the rate of 15 sec/layer. In C3S system, the paving blade is not required to go backwards to initiate paving the new layer; this cuts down the drying time starting from the first cycle of slurry paving. Unlike the linear 3S system, where the paving blade needs to wait until the paved layer dries and returns to its origin.

Figure 7 (a), (b) & (c) represents the flow chart of the fabrication of green parts. Initially, the slurry is deposited on the build platform and a paving blade paves the slurry in the form of a ring as shown in 7(a). Next, the masking light is projected by the DLP systems, which is P2 and P5 in this case. The masking light is exposed for 0.7 sec each layer for curing. Finally, the build platform is removed from the system and the green parts are washed with water until the uncured slurry is gone.

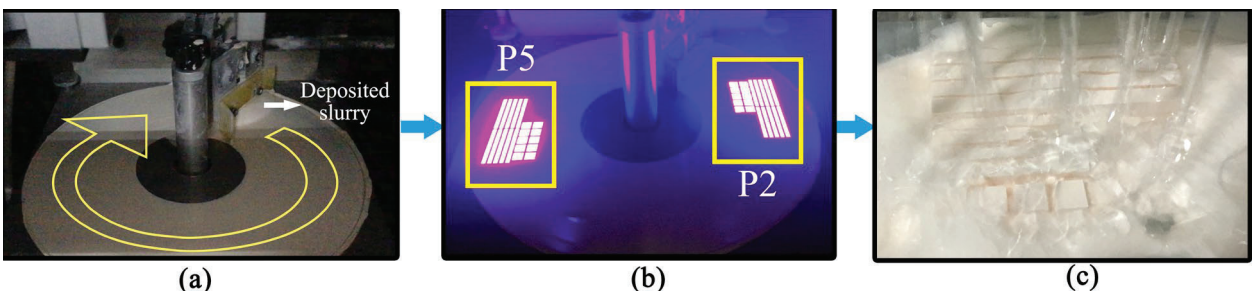

Figure 7: (a) Paving of the deposited slurry on the build platform (b) P2 and P5 projectors exposing the masking light (c) Post processing the green parts under running water

Table 1 shows the data of the dimensions of the green parts obtained after 3D printing. The design sample is 6mm x 6mm x 1.8mm. The green parts obtained from the experiment with 15 sec/layer printing speed exhibited bigger dimensions than the parts obtained from 30 sec/layer printing speed experiment. It is due to the vaporization of the solvent from a paved layer, causes increase in vol % of the dye. At low printing speeds the vaporized solvent is high at high printing speeds. The increase in vol % of dye decreases the penetration of light through the paved layer. Hence, at the same exposure time of masking light, the parts printed at 15 sec/layer penetrate more light energy than parts printed at 30 sec/layer. More light energy can cause over curing and more diffuse scattering, which results in increase in the dimensional errors.

Table 1: Dimensions of the green parts

	15 sec/layer			30 sec/layer		
Sample	Length (mm)	Width (mm)	Thickness (mm)	Length (mm)	Width (mm)	Thickness (mm)
1	6.24	6.24	1.93	6.03	6.09	1.86
2	6.07	6.12	1.97	5.95	5.95	1.83
3	6.18	6.11	1.92	6.00	6.02	1.87
4	6.06	6.11	1.94	6.03	6.02	1.86

5	6.13	6.11	1.94	6.02	5.94	1.83
6	6.10	6.11	1.94	5.90	5.93	1.81
7	6.10	6.07	1.92	5.87	5.90	1.85
8	6.12	6.10	1.94	6.10	6.04	1.87
Average	6.125	6.121	1.938	5.988	5.986	1.848
Deviation	0.052	0.044	0.014	0.067	0.058	0.019

2.4. Debinding and sintering of the green parts

Debinding is the process of removing the binder from the green parts. The debinding is done by subjecting the green parts to heating up to 350 ℃ at the rate of 3.4 ℃/min for 1 h 30 min and then from 350 ℃ to 600 ℃ at the rate of 0.92 ℃/min for 4 h 30 min. This is followed by a sintering process, which is done by heating the parts up to 1600 ℃ at the rate of 1.6 ℃/min. At 1600 ℃, the green parts become highly densified and exhibit pure ceramic properties. The parts are left at 1600 ℃ for two hours to let the densification process complete. After densification, the objects are cooled down to 40 ℃ at the rate of 2.8 ℃/min for 9 hours. Figure 8 (a) represents the debinding and sintering cycle of the green parts and (b) shows the green parts kept inside ceramic containers ready for sintering.

(a) (b)

Figure 8: (a) Debinding and sintering cycle (b) Sintering of green parts

Table 2 shows the dimensional data of the sintered samples. From the data, it is observed that the dimensions of the low speed printed parts are less than the parts printed at high speed.

Table 2: Dimensional data of the sintered parts

Sample	15 sec/layer (high speed)			30 sec/layer (low speed)		
	Length (mm)	Width (mm)	Thickness (mm)	Length (mm)	Width (mm)	Thickness (mm)
1	4.86	4.86	1.58	4.82	4.85	1.45
2	4.85	4.82	1.54	4.92	4.89	1.51
3	4.83	4.89	1.51	4.8	4.84	1.47
4	4.87	4.9	1.47	4.86	4.87	1.49

5	4.84	4.85	1.50	4.77	4.78	1.52
6	4.84	4.88	1.54	4.82	4.86	1.5
7	4.81	4.83	1.59	4.77	4.84	1.51
8	4.83	4.81	1.52	4.84	4.82	1.53
Average	4.841	4.855	1.531	4.825	4.844	1.498
Deviation	0.017	0.029	0.035	0.044	0.029	0.023

3. Characterization of the samples printed at different layer cycle time

In this paper, the mechanical properties are characterized by printing the sample parts at different speeds with the same slurry material. The printing speeds are 15 seconds/ layer (high speed) and 30 seconds/layer (low speed). 3D model of blocks with 6mm in length and width and thickness of 1.8 mm are 3D printed to determine the shrinkage rate, average volume and density. To determine the flexural strength, rectangular bars with dimensions 30×2.4×1.8 mm in length, width, and thickness respectively, are fabricated. The printed green parts and the sintered parts of 3D models are as shown in the figure 9 (a) and (b).

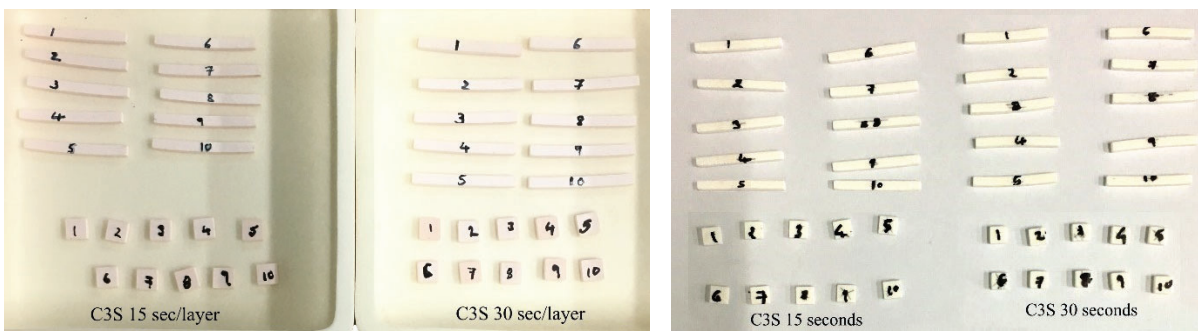

(a) (b)

Figure 9: (a) Green parts (b) Sintered parts

3.1. Shrinkage rate

The dimensions of the obtained green parts are measured under the 3D macroscope. The table 1 represents the length, width and thickness of the green parts obtained from C3S printing with 15 sec/layer and 30 sec/layer. From the table 3 the shrinkage rate of the parts printed at 30 sec/layer speed is slightly lesser than the parts printed at 15 sec/layer speed. The shrinkage is almost linear in the X, Y and Z directions with slight error in length of the parts printed at low speed. The mean shrinkage rate of the parts printed at 15 sec/layer is 20.95 × 20.68 × 20.96 % and the parts printed at 30 sec/layer is 19.41 × 19.08 × 18.93 % in X, Y and Z directions respectively. Comparatively, the low speed printed parts exhibited the low shrinkage rate due to the occurrence of high solid loading with increased amount of solvent vaporization every layer while printing.

Table 3: Shrinkage rate of the samples after sintering

Sample	15 sec/layer	30 sec/layer

	Length (%)	Width (%)	Thickness (%)	Length (%)	Width (%)	Thickness (%)
1	22.115	22.115	18.135	20.066	20.361	22.043
2	20.099	21.242	21.827	17.311	17.815	17.486
3	21.845	19.967	21.354	20.000	19.601	21.390
4	19.637	19.804	24.227	19.403	19.103	19.892
5	21.044	20.622	22.680	20.764	19.529	16.940
6	20.656	20.131	20.619	18.305	18.044	17.127
7	21.148	20.428	17.188	18.739	17.966	18.378
8	21.078	21.148	21.649	20.656	20.199	18.182
Average	20.953	20.682	20.960	19.406	19.077	18.930
Deviation	0.727	0.686	2.037	1.067	0.899	1.727

3.2. Density

The density of the samples is measured using a densimeter that follows Archimedes principle. The obtained mean density value of the eight samples is measured as 3.846 g/cm^3 for 15 sec/layer and 3.874 g/cm^3 for 30 sec/layer speed. From the data presented in table 4, the density of the low speed printed parts is 0.028 g/cm^3 higher than the high speed printed parts. This variation is due to the increase in solid loading every layer. At low speed printing, the vaporization of solvent is high causing the solid particles to come closer and hence fixated at the masking light with a higher density. Whereas at high-speed printing, the presence of solvent is relatively high and caused the solid loading little lesser. The difference in standard deviations for high speed and low speed printing is also very high. The inconsistency of density in high-speed printed parts is due to presence of internal cracks or pores in few of the samples. Whereas in low speed printed parts the density values are consistent causing lower standard deviation.

Table 4: Density of the samples after sintering

Sample	15 sec/layer	30 sec/layer
1	3.67	3.86
2	3.99	3.79
3	4.04	3.96
4	3.83	3.81
5	3.64	3.91
6	3.98	3.84
7	3.96	3.96
8	3.66	3.86
Average	3.846	3.874
Deviation	0.157157	0.059987

3.3. Flexural strength

The flexural strength of the workpieces is measured by the 3-point bending test as shown in figure 10, which is based on the ASTM C1161 standards. In order to obtain the final 3D printed parts with the dimensions of 25×2×1.5 mm length, width and depth respectively, the shrinkage rate is predicted to be 20% and hence the 3D model with 30×2.4×1.8 mm in length, width and depth is 3D printed and sintered. The obtained final parts are in the tolerances mentioned as per the ASTM C1161 standards. The mean flexural strength obtained for the eight rectangular bars is measured to be 367.72 MPa, 418.29 MPa for parts printed at 15 sec/layer and 30 sec/layer speeds. The table 5 shows the results of the 3-point bending test on the printed samples. The difference in the flexural strengths is due to the higher density of the obtained samples at low speed printing.

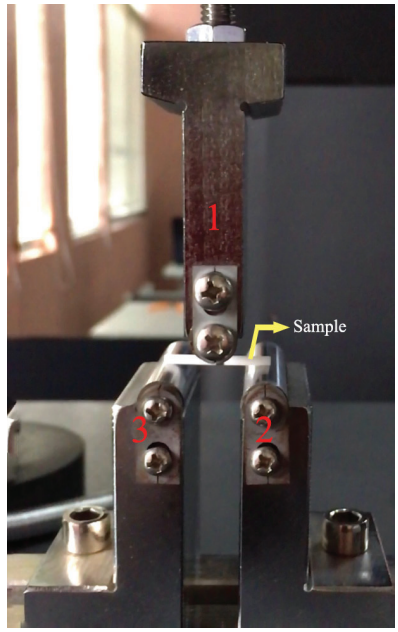

Figure 10: 3-point bending test

Table 5: Characterization of the sintered samples

Sample	15 sec/layer	30 sec/layer
1	339.11	455.51
2	339.49	432.46
3	451.44	335.03
4	300.64	415.17
5	378.42	319.89
6	423.97	373.06
7	396.99	461.58
8	311.73	489.82
Average	367.72	410.32
Deviation	47.60	54.51

4. Discussion

The C3S system is operated at two different printing speeds i.e. at 15 sec/layer and 30 sec/layer. At high printing speed, the fabrication of the green parts is reduced to half the time it usually takes. However, the mechanical characteristics for the parts printed at low speed exhibited better results compared to the parts printed at high speed. Due to the high vaporization of solvent in low speed printed parts, it resulted in high solid loading and higher density of the parts, 3.87 g/cm^3 whereas it is 3.84 g/cm^3 at higher speed. In addition, the flexural strength of the parts printed at low speed is 410.32 MPa, which is ~42 MPa higher than the parts printed at high speed. For a 6×6×1.8 mm 3D model, after printing at high and lower speeds, the dimensional error in the green parts is measured to be comparatively lesser in the low speed printed parts. It is due to the raise in dye vol % when the solvent is vaporized at a proportional rate of the paving time for every layer. The masking light scattering is inversely proportional to the vol % of dye. Hence, the dimensional error that is caused due to overcuring is lesser in low speed parts. To obtain green parts with exact dimensions of the 3D model, the printing speed time can be optimized. Although it is impractical to achieve parts with exact dimensions as 3D model, the parts can be printed within the standard tolerances.

5. Conclusion

A new C3S system is developed based on the same working principle as 3S to increase the productivity. The new apparatus is suitable for small-scale and batch wise production processes. By implementing two projectors in the C3S, the productivity has been increased 4 times; counting the printing speed when reduced to half. The new C3S is capable of printing at different speeds effectively. The mean shrinkage rate of the parts is 20.95 × 20.68 × 20.96 % and 19.41 × 19.08 × 18.93 % in X, Y and Z directions respectively for the parts printed at 15 sec/layer and 30 sec/layer. The parts printed at 15 sec/layer speed exhibited flexural strength of 367 MPa, 3.84 g/cm^3 density; parts printed at 30 sec/layer speed exhibited flexural strength of 418 MPa, density of 3.87 g/cm^3. The layer resolution remains the same while the mechanical properties depends upon the chosen printing speed. To increase the productivity and make an AM system that is suitable for batch production, the C3S can be utilized to its full potential by implementing up to six projectors in one system.

References:

Dizon, J. R. C. *et al.* (2018) 'Mechanical characterization of 3D-printed polymers', *Additive Manufacturing*. Elsevier B.V., 20, pp. 44–67. doi: 10.1016/j.addma.2017.12.002.

Frazier, W. E. (2014) 'Metal additive manufacturing: a review', *Journal of Materials Engineering and Performance*. Springer, 23(6), pp. 1917–1928.

He, R. *et al.* (2018) 'Fabrication of complex-shaped zirconia ceramic parts via a DLP-stereolithography-based 3D printing method', *Ceramics International*, 44(3), pp. 3412–3416. doi: 10.1016/j.ceramint.2017.11.135.

Hu, K. *et al.* (2018) 'Design of a Shaping System for Stereolithography with High Solid Loading Ceramic Suspensions', *3D Printing and Additive Manufacturing*, 00(00), p. 3dp.2017.0065. doi: 10.1089/3dp.2017.0065.

Lee, H. D. *et al.* (1986) 'Photopolymerizable binders for ceramics', *Journal of materials science*

letters. Springer, 5(1), pp. 81–83.

Ligon, S. C. *et al.* (2017) 'Polymers for 3D Printing and Customized Additive Manufacturing', *Chemical Reviews*, 117(15), pp. 10212–10290. doi: 10.1021/acs.chemrev.7b00074.

Liu, K. *et al.* (2013) 'Densification of alumina components via indirect selective laser sintering combined with isostatic pressing', *International Journal of Advanced Manufacturing Technology*, 67(9–12), pp. 2511–2519. doi: 10.1007/s00170-012-4668-0.

Schwentenwein, M. and Homa, J. (2015) 'Additive manufacturing of dense alumina ceramics', *International Journal of Applied Ceramic Technology*, 12(1), pp. 1–7. doi: 10.1111/ijac.12319.

Tang, H. H., Chiu, M. L. and Yen, H. C. (2011) 'Slurry-based selective laser sintering of polymer-coated ceramic powders to fabricate high strength alumina parts', *Journal of the European Ceramic Society*. Elsevier Ltd, 31(8), pp. 1383–1388. doi: 10.1016/j.jeurceramsoc.2011.02.020.

Wang, J.-C. and Dommati, H. (2018) 'Fabrication of zirconia ceramic parts by using solvent-based slurry stereolithography and sintering', *The International Journal of Advanced Manufacturing Technology*. The International Journal of Advanced Manufacturing Technology. doi: 10.1007/s00170-018-2349-3.

Wang, J. C. (2013) 'A novel fabrication method of high strength alumina ceramic parts based on solvent-based slurry stereolithography and sintering', *International Journal of Precision Engineering and Manufacturing*, 14(3), pp. 485–491. doi: 10.1007/s12541-013-0065-3.

Wang, J., Dommati, H. and Hsieh, S.-J. (2019) 'Review of additive manufacturing methods for high-performance ceramic materials', *The International Journal of Advanced Manufacturing Technology*. Springer, pp. 1–21.